The linear theory of the circular free-electron laser

H. Saito[a] and J. S. Wurtele
Plasma Fusion Center, Massachusetts Institute of Technology, Cambridge, Massachusetts 02139

(Received 18 July 1986; accepted 6 April 1987)

A small signal theory of a free-electron laser (FEL) with a rotating electron beam in a uniform axial magnetic field and in an azimuthal wiggler field (the "circular" FEL) is developed. The analysis includes the low and high gain regimes and the influence of longitudinal space-charge forces. It is found that the circular FEL instability has two regimes: a strong pump regime and a negative mass dominated regime. The negative mass regime replaces the weak pump (Raman) regime found for the usual FEL geometry in which the electron beam propagates in the axial direction (the "linear" FEL). The dispersion relation is evaluated, and the resulting growth rates are compared with those of the linear FEL. For a cold beam, at fixed output frequency, the growth rate in the strong pump regime is larger, by a factor of $\gamma^{2/3}$, in the circular FEL. The negative mass instability is shown to increase the growth rate and modify the bandwidth of the circular FEL in the strong pump regime. However, the circular FEL performance is found to be more sensitive to the energy spread than the linear FEL.

I. INTRODUCTION

A new type of free-electron laser, the "circular" free-electron laser (FEL), has been theoretically[1–3] and experimentally[4,5] investigated. As originally proposed by Bekefi,[1] the magnetic field configuration consists of a uniform axial field $B_0\hat{z}$ and an azimuthally periodic wiggler field $\mathbf{B}_w(r,\theta)$. The relativistic electron beam rotates azimuthally and wiggles axially, as shown in Fig. 1. Such a wiggler field is generated by an assembly of magnets placed behind two concentric metal cylinders. Near the center of the gap the wiggler magnetic field is primarily radial and is transverse to the electron flow velocity. The metallic boundaries act as a coaxial waveguide for the radiation. The conventional FEL geometry, in which the electron beam propagates axially and wiggles in the transverse plane, will be referred to here as a "linear" FEL.

Yin and Bekefi[3] derived the dispersion relation for the circular FEL in the strong pump, high gain regime. Their analysis used a fluid model and did not include longitudinal space charge or energy spread. Here we extend their work by developing a one-dimensional nonlinear model that includes space charge, energy spread, and the transverse profile of coaxial waveguide modes. Our model is similar to the description of the linear FEL presented by Kroll, Morton, and Rosenbluth and others.[6–8]

In this paper we analytically solve for the gain characteristics of the circular FEL in the low gain limit and in the high gain strong and weak pump limits. Linearization of the equations of motion for the circular FEL, in the small signal regime, results in a cubic dispersion relation. This cubic is then compared to the cubic resulting from the small signal analysis of the linear FEL.[9,10] At fixed frequency, in the cold beam, strong pump regime, the growth rate of the circular FEL is larger by a factor of $\gamma^{2/3}$ than that of the linear FEL. Unfortunately, the circular FEL has a greater sensitivity to energy spread than does the linear FEL. We find that the negative mass instability can significantly influence the growth rate of the circular FEL. In particular, there is no equivalent to the Raman regime in the circular FEL. Instead, as the beam current is increased the negative mass instability dominates and the growth rate becomes independent of the pump field strength.

In an experimental realization of the circular FEL, the electron beam will have a small axial velocity. After a large number of azimuthal revolutions the beam will exit the wiggler. The radiation, which is in a coaxial waveguide mode, exits the waveguide because of a small parallel component of $\mathbf{k}$ ($\beta_\perp/\beta_\parallel \sim k_\perp/k_\parallel$). It should be possible to taper the wiggler field amplitude, as a function of axial position and, thereby, to increase the efficiency of the laser. In our treatment we use a one-dimensional model that ignores the parallel motion; analytic treatment of a tapered circular FEL must await a three-dimensional analysis.

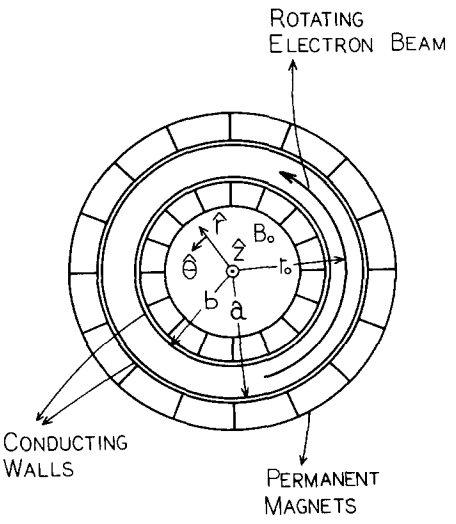

FIG. 1. Configuration of the circular FEL.

[a] Present address: Institute of Space and Astronautical Science, Tokyo, Japan.

 0031-9171/87/072209-12$01.90

Section II contains the derivation of a nonlinear, one-dimensional model for the circular FEL. In Sec. III the low gain regime is examined, and in Sec. IV the exponential gain dispersion relation is derived and studied. We briefly discuss optimization in Sec. V, and Sec. VI contains some conclusions.

II. THEORETICAL MODEL

A. Wiggler and electromagnetic fields

The configuration of the circular free-electron laser is shown in Fig. 1. A uniform magnetic field $\mathbf{B}_0 = B_0\hat{z}$ is applied in the axial (z) direction. The corresponding vector potential is given by $\mathbf{A}_0 = (B_0 r/2)\hat{\theta}$. The wiggler field $\mathbf{B}_w$ is given by[3]

$$\mathbf{B}_w(r,\theta) = -\hat{r}\frac{\tilde{B}_w}{2}\sin(N\theta)\left[\left(\frac{r}{a'}\right)^{N-1}+\left(\frac{b'}{r}\right)^{N+1}\right]\times\left(\frac{a'}{b'}\right)^{(N^2-1)/2N}+\hat{\theta}\frac{\tilde{B}_w}{2}\cos(N\theta)\times\left[\left(\frac{r}{a'}\right)^{N-1}-\left(\frac{b'}{r}\right)^{N+1}\right]\left(\frac{a'}{b'}\right)^{(N^2-1)/2N}, \tag{1}$$

where a' and b' denote the radii of the outer and inner magnetic surface, N is the number of wiggler periods, and $\tilde{B}_w$ is the amplitude of the wiggler field. We adjust the radii a' and b' so that the azimuthal component of $\mathbf{B}_w$ vanishes at the electron-beam radius $r_0 = (a'^{N-1}b'^{N+1})^{1/2N}$. The wiggler field can then be approximated by

$$\mathbf{B}_w = -\tilde{B}_w(r_0/r)\sin N\theta\hat{r} \tag{2}$$

near $r = r_0$. The corresponding vector potential of the wiggler field is

$$\mathbf{A}_w = (\tilde{B}_w r_0/N)\cos N\theta\hat{z}. \tag{3}$$

The radiation mode of the circular FEL is a coaxial waveguide mode that is a traveling wave in the azimuthal direction. Since the electrons are assumed to have no axial streaming velocity, $k_z = 0$ corresponds to the case where the growth rate of the FEL instability is the largest.[3] The coupling between the axial electric field (E_z) and the oscillatory axial velocity (v_z), because of the wiggler field, results in the FEL interaction. The radiation mode must be transverse magnetic (TM), since only TM modes have axial components of the electric field. However, the ponderomotive potential of FEL causes bunching of electron beams in the azimuthal direction and thereby drives a longitudinal space-charge wave.

The vector potential $\mathbf{A}_s$ of the TM mode radiation is

$$\mathbf{A}_s(\mathbf{r},t) = -\tilde{A}_s(r,t)\cos(p\theta-\omega_s t+\phi_s)\hat{z}, \tag{4}$$

and the axial electric field E_z corresponding to $\mathbf{A}_s$ is

$$E_z(\mathbf{r},t) = -\omega_s\tilde{A}_s(r,t)\sin(p\theta-\omega_s t+\phi_s). \tag{5}$$

We assume $d\tilde{A}_s/dt \ll \omega_s\tilde{A}_s$. The radial dependence $\tilde{A}_s(r,t)$ is given by

$$\tilde{A}_s(r,t) = M(t)X_p(k_r r), \tag{6}$$

where M denotes the time-dependent field amplitude. The function X_p is

$$X_p(k_r r) = Y_p(k_r a)J_p(k_r r) - J_p(k_r a)Y_p(k_r r), \tag{7}$$

where J_p and Y_p are the first and second kind of Bessel function, respectively.[11] In Eq. (7) p is the mode number in the azimuthal direction. The radial wavenumber k_r is determined by solving $X_p(k_r b) = 0$. The coaxial waveguide modes are labeled TM_{pq}, where the index q refers to the qth zero of $X_p(k_r b) = 0$. At cutoff, $k_z = 0$ and $k_r = \omega_s/c$.

The energy density U and the circulating power P (Poynting power in the azimuthal direction) of the TM_{pq} mode radiation per unit axial length are given by

$$U = (\pi/2)\epsilon_0 M^2[a^2X_p'(k_r a)^2 - b^2X_p'(k_r b)^2], \tag{8}$$

$$P = \left(\frac{\epsilon_0 c}{4k_r}\right)M^2\left(X_{p,0}(k_r r)^2 - 2\sum_{\nu=0}^{p-1}X_{p,\nu}(k_r r)^2\right)\Bigg|_{r=b}^{r=a}, \tag{9}$$

where $X_{p,\nu}(k_r r)$ is defined as

$$X_{p,\nu}(k_r r) = Y_p(k_r a)J_\nu(k_r r) - J_p(k_r a)Y_\nu(k_r r). \tag{10}$$

B. Nonlinear equations

An annular relativistic electron beam with infinitely small thickness is introduced in the gap at $r = r_0$, where the azimuthal component of the wiggler field $\mathbf{B}_w$ vanishes. The electrons are subject to the cyclotron motion, which is slightly perturbed by the wiggler and the radiation. We have the simple relation

$$(\omega_c/\gamma)r_0 = c\beta, \tag{11}$$

where $\omega_c = eB_0/m$ and B_0 is the amplitude of the uniform axial magnetic field. Here $\beta = v/c$ and $\gamma = (1-\beta^2)^{-1/2}$, where v is the electron velocity.

Neither the wiggler field nor the cutoff radiation mode vary in the axial (z) direction. Therefore the z component of the canonical momentum is conserved and the axial velocity v_z is given by

$$v_z = (c/\gamma)\sqrt{2}[a_w\cos N\theta - |a_s|\cos(p\theta-\omega_s t+\phi_s)], \tag{12}$$

where $a_w = (er_0\tilde{B}_w/\sqrt{2}mcN)$ and $|a_s| = (e/\sqrt{2}mc)\times\tilde{A}_s(r_0,t)$.

For the electrons that are subject to the concentric motion in the uniform and the wiggler field, the radial component of the canonical momentum is conserved to order (a_w/γ). The radial variation of the wiggler field and waveguide mode is neglected. This approximation requires an annular electron beam and places constraints on the beam energy spread, which are discussed in Sec. IV D. Under the further assumption that the wiggler field only slightly perturbs the electron motion, $(a_w/\gamma)^2 \ll 1$, we expect the radial velocity to vanish:

$$v_r = 0. \tag{13}$$

Note that there is no radial component to the vector potential. To obtain the azimuthal component v_θ of the electron velocity, we use Eqs. (12) and (13) and the definition of γ. Thus

$$v_\theta = c\beta\{1-(2/\gamma^2\beta^2)[a_w\cos N\theta - |a_s|\cos(p\theta-\omega_s t+\phi_s)]^2\}^{1/2}. \tag{14}$$

We now define the electron phase ζ as

$$\zeta = (p+N)\theta - \omega_s t. \tag{15}$$

Using (11) and (14), the electron angular velocity defined by $d\theta/dt = v_\theta/r_0$ is

$$\frac{d\theta}{dt} = \frac{\omega_c}{\gamma}\left(1 - \frac{1}{2\gamma^2}\left[a_w^2 - 2|a_s K_B| a_w \cos(\zeta + \phi_s)\right]\right), \tag{16}$$

where we averaged $d\theta/dt$ over a wiggler period and used $\beta \approx 1$ and $|a_s| \ll a_w$. The factor $K_B = J_0(R) - J_1(R)$, where $R = a_w^2/2(1+a_w^2)$, is analogous to a similar factor found for plane polarized linear wigglers.[7]

The electron phase ζ evolves according to Eqs. (15) and (16):

$$\frac{d\zeta_j}{dt} = \frac{1}{2}\left[(p+N)\frac{\omega_c}{\gamma_j}\left(1 - \frac{1}{2\gamma_j^2} \times (a_w^2 - 2a_s K_B a_w e^{i\zeta_j})\right) + \text{c.c.}\right] - \omega_s, \tag{17}$$

where the index j has been introduced as an electron label and the complex representation $a_s = |a_s| e^{i\phi_s}$ is used. Here c.c. denotes complex conjugate. By setting $d\zeta/dz = 0$ for an electron with the average beam energy, γ_0, the FEL resonant frequency is found to be

$$\omega_0 = (p+N)(\omega_c/\gamma_0)(1 - a_w^2/2\gamma_0^2). \tag{18}$$

The electron energy evolves according to

$$\frac{d\gamma_j}{dt} = \frac{1}{2}\left(i\omega_s a_s K_B a_w \frac{e^{i\zeta_j}}{\gamma_j} + \text{c.c}\right) + \left(\frac{f_1 \omega_p^2}{i(p+N)\omega_c/\gamma_j}\langle e^{-i\zeta}\rangle e^{i\zeta_j} + \text{c.c.}\right), \tag{19}$$

where the symbol $\langle\ \rangle$ means an average over the electron distribution. In Eq. (19) ω_p is the plasma frequency defined by

$$\omega_p^2 = e^2 N_e/m\epsilon_0\pi(a^2 - b^2). \tag{20}$$

Here N_e is the number of electrons per unit axial length. The first term on the right-hand side in Eq. (19) is the ponderomotive force produced by the wiggler and radiation fields, and the second term is from the longitudinal space-charge force.[9,10] For the circular FEL, when the geometric factor f_1 [described in Eq. (21)] is positive, the system has a negative mass instability.[12–15] This instability results from the azimuthal bunching induced by the FEL interaction. The coupling factor f_1, which includes the influence of the waveguide on the negative mass instability, is given by[14]

$$f_1 = g(p+N)\left[(a^2 - b^2)/4r_0^2\right], \tag{21}$$

where

$$g = \left[(b_+ + b_-)/2 + (p+N)(\Delta r/r_0)\right]^{-1}. \tag{22}$$

The quantity Δr is the half-width of the electron beam and $b_\pm$ denote the wave admittance and are discussed in the Appendix. As will be shown in Sec. IV B, a small signal analysis of Eqs. (17) and (19) yields, in the absence of the wiggler field, the well-known growth rate for the negative mass instability.[14]

The evolution of the slowly varying amplitude, $a_s(t)$, is found by inserting Eq. (4) into the wave equation. Following the standard treatment of the linear FEL in a waveguide,[10] the wave equation is next multiplied by the mode factor $rX_p(k_r r)$ [Eq. (7)] and integrated over the radial coordinate ($b < r < a$). Averaging over a wiggler period then yields the desired equation,

$$\frac{da_s}{dt} = if_2 \frac{\omega_p^2 K_B a_w}{2\omega_s}\left\langle \frac{e^{-i\zeta}}{\gamma}\right\rangle. \tag{23}$$

The coupling factor for the mode, f_2, using well-known orthogonality relations of Bessel functions,[11] is

$$f_2 = \frac{(a^2 - b^2)X_p^2(k_r r_0)}{a^2 X_p'^2(k_r a) - b^2 X_p'^2(k_r b)}. \tag{24}$$

We recall that k_r is the radial wavenumber of the TM_{pq} mode and f_2 depends on the mode, the waveguide geometry, and the beam position. When the azimuthal mode number p is small enough, the radial profile $X_p(k_r r)$ of the field is approximately sinusoidal and f_2 is then

$$f_2 = [(a+b)/r_0]\sin k_r(a - r_0), \tag{25}$$

where $k_r \simeq \pi q/(a-b)/2$. When the electron beam is near the center of the gap, $r_0 \approx (a+b)/2$, Eq. (25) reduces to $f_2 \simeq 2$ for odd q, and $f_2 \simeq 0$ for even q.

In summary, we have a complete set of the equations that describe the circular FEL. Equations (17) and (19) govern the electron motions, and Eq. (23) is the self-consistent wave equation.

C. Comparison with the linear FEL

Before analyzing the small signal theory of the circular FEL, we compare the equations of evolution of the circular FEL with those of the conventional linear FEL. We consider a linear FEL with the ideal wiggler field $\mathbf{B}_w = -\tilde{B}_w \sin k_w z \hat{x}$ and with no guiding axial magnetic field. The velocity dz/dt of the electron is given by

$$\frac{dz}{dt} = c\left(1 - \frac{1}{2\gamma^2}\left[1 + a_w^2 - (a_s K_B a_w e^{i\zeta} + \text{c.c.})\right]\right). \tag{26}$$

For the linear FEL, the electron equations of motion are

$$\frac{d\zeta_j}{dt} = \frac{1}{2}\left[c(k+k_w)\left(1 - \frac{1}{2\gamma^2} \times (1 + a_w^2 - 2a_s K_B a_w e^{i\zeta_j})\right) + \text{c.c.}\right] - \omega_s, \tag{27}$$

$$\frac{d\gamma_j}{dt} = \frac{1}{2}\left(i\omega_s a_s K_B a_w \frac{e^{i\zeta_j}}{\gamma_j} + \text{c.c.}\right) + \left(\frac{f_{1L}\omega_p^2}{i(k+k_w)c}\langle e^{-i\zeta}\rangle e^{i\zeta_j} + \text{c.c.}\right), \tag{28}$$

where k and k_w denote the wavenumber of the radiation and the wiggler field, and the electron phase is defined by $\zeta = (k+k_w)z - \omega_s t$. The resonance condition for the linear FEL is

$$\omega_0 = c(k + k_w)\left[1 - (1/2\gamma_0^2)(1 + a_w^2)\right]. \quad (29)$$

The wave equation of the linear FEL is identical to that of the circular FEL, Eq. (23), except that the spatial coupling factor f_2 is replaced by the corresponding coupling factor f_{2L}. The factor f_{2L} depends on transverse geometry and the overlap between the electron beam and the radiation mode. The appropriate coupling factors for the longitudinal space-charge field (f_{1L}) and the electromagnetic mode (f_{2L}) have been discussed elsewhere.[10]

The wavenumbers of the radiation and the wiggler fields for the circular FEL are defined as

$$k = p/r_0, \quad (30)$$

$$k_w = N/r_0. \quad (31)$$

From Eq. (11) and the definitions of k and k_w, we find

$$(p + N)(\omega_c/\gamma) = c(k + k_w)(1 - 1/2\gamma^2), \quad (32)$$

where $\gamma^2 \gg 1$ is used. Equation (32) can be used to show that Eqs. (17), (19), and (18) for the circular FEL are "formally" identical to those Eqs. (27), (28), and (29) for the linear FEL.

The synchronous phase ζ evolves according to Eq. (17) for the circular FEL and Eq. (27) for the linear FEL. The different energy dependences in Eqs. (17) and (27) result from using $d\theta/dt$ (dz/dt) in the definition of ζ for the circular (linear) FEL. Among the consequences of this are differences in the growth rates and efficiencies of the FEL's.

The vacuum waveguide dispersion relation in a linear FEL is

$$\omega^2 = c^2k^2 + \omega_{\text{cut}}^2, \quad (33)$$

where k is the axial wavenumber and ω_{cut} is the cutoff frequency. For the coaxial waveguide of the circular FEL, with $(a - b)/a \ll 1$, the vacuum dispersion relation is approximately[11]

$$\omega^2 = (\omega_+ p)^2 + (\omega_-^2 q^2 - \omega_+^2/4), \quad (34)$$

where $\omega_+ = 2c/(a + b)$ and $\omega_- = \pi c/(a - b)$. If the electron beam is near the midpoint of the gap [$r_0 \simeq (a + b)/2$], then $\omega_+ p \simeq ck$, where $k = p/r_0$ is the wavenumber. Equation (34) is then in the same form as Eq. (33), with $(\omega_-^2 q^2 - \omega_+^2/4)^{1/2}$ considered the "cutoff frequency" in the azimuthal direction.

III. THE LOW GAIN REGIME

This section examines the circular FEL in the low gain regime. We assume a cold, tenuous electron beam and therefore neglect the space-charge term in Eq. (19). Each electron has the same initial energy γ_0 and the different initial phase ζ. We drop the label j in this section. Since the gain is low, the radiation can be considered constant. Equations (17) and (19) become

$$\frac{d\zeta}{dt} = (p + N)\frac{\omega_c}{\gamma}\left(1 - \frac{a_w^2}{2\gamma^2}\right) - \omega_s, \quad (35)$$

$$\frac{d\gamma}{dt} = -\frac{\omega_s |a_s| K_B a_w}{\gamma} \sin\zeta. \quad (36)$$

Linearizing Eqs. (35) and (36), with $\delta\gamma = \gamma - \gamma_0$ and with γ_0 the initial beam energy, yields

$$\frac{d\zeta}{dt} = \Delta\omega + Q\delta\gamma, \quad (37)$$

$$\frac{d\delta\gamma}{dt} = -\epsilon \sin\zeta, \quad (38)$$

where $\epsilon \equiv \omega_s |a_s| K_B a_w/\gamma_0$, the frequency detuning $\Delta\omega \equiv \omega_0 - \omega_s$, $\omega_0 \equiv (p + N)(\omega_c/\gamma_0)(1 - a_w^2/2\gamma_0^2)$, and $Q \equiv -(p + N)(\omega_c/\gamma_0^2)(1 - 3a_w^2/2\gamma_0^2)$.

For the linear FEL, a similar analysis of Eqs. (27) and (28) yields equations of the same form as Eqs. (37) and (38), except that the coefficients are now $\omega_0 \equiv c(k + k_w) \times [1 - (1/2\gamma_0^2)(1 + a_w^2)]$ and $Q \equiv c(k + k_w)\gamma_0^{-3} \times (1 + a_w^2)$.

Using the wavenumbers k and k_w of the circular FEL defined in Sec. II C, we find that ϵ, $\Delta\omega$, and ω_0 are identical for the circular FEL and the linear FEL. Only Q is different:

$$Q \simeq \begin{cases} -\omega_0/\gamma_0 & \text{(circular FEL)}, \\ (\omega_0/\gamma_0^3)(1 + a_w^2) & \text{(linear FEL)}. \end{cases} \quad (39)$$

With $\Delta\omega = 0$, the Hamiltonian H for Eqs. (37) and (38) is

$$H(\delta\gamma, \zeta) = \tfrac{1}{2} Q(\delta\gamma)^2 - \epsilon \cos\zeta, \quad (40)$$

where $\epsilon = \omega_s |a_s| K_B a_w/\gamma_0$ both for the circular and the linear FEL, and Q is defined in Eq. (39). Equation (40) allows us to interpret Q as the inverse of the mass of a particle trapped by the potential well. In this analogy, the circular FEL has a "negative mass," the absolute value of which is "lighter" than that of the linear FEL by a factor of γ_0^2.

The height $\delta\gamma_m = 2(\epsilon/|Q|)^{1/2}$ of the ponderomotive potential is given by

$$\delta\gamma_m = \begin{cases} 2\sqrt{|a_s| K_B a_w} & \text{(circular FEL)}, \\ 2\gamma_0\sqrt{|a_s| K_B a_w/(1 + a_w^2)} & \text{(linear FEL)}. \end{cases} \quad (41)$$

The synchrotron frequency $\Omega = (\epsilon|Q|)^{1/2}$ in the ponderomotive potential is

$$\Omega = \begin{cases} (\omega_0/\gamma_0)\sqrt{|a_s| K_B a_w} & \text{(circular FEL)}, \\ (\omega_0/\gamma_0^2)\sqrt{|a_s| K_B a_w (1 + a_w^2)} & \text{(linear FEL)}. \end{cases} \quad (42)$$

Equations (37) and (38) can be used to solve for the gain in the same way as in the linear FEL.[7] We define the energy gain G as the ratio between the loss of electron energy and the energy of the radiation field [Eq. (8)]. The gain of the circular FEL as a function of time is

$$G(t) = \frac{\omega_p^2 \omega_0}{\gamma_0^3} K_B^2 a_w^2 \left(\frac{t}{2}\right)^3 f_2 h\left(\frac{\Delta\omega t}{2}\right), \quad (43)$$

where h denotes the spectrum function $h(x) \equiv d/dx(\sin x/x)^2$, and the spatial coupling factor f_2 is given in Eq. (24).

The well-known formula for the corresponding gain of the linear FEL in the low gain regime is shown in Table I. The gain is proportional to Q, and hence the gain of the circular FEL is larger than that of the linear FEL by a factor of γ^2. Also, the spectrum shape is inverted with respect to $\Delta\omega_0 = 0$. A similar "inverted spectrum shape" is found[16] in a particular parameter region of a linear FEL with a helical wiggler and an axial magnetic field.

TABLE I. Gain and efficiency of circular and linear FEL's.

	Circular FEL		Linear FEL	
	Growth rate ω_i	Efficiency η	Growth rate ω_i	Efficiency η
Low gain regime	$G = f_2 K_B^2 \omega_p^2 \omega_0 \gamma^{-3} a_w^2 (t/2)^3 h$	...	$G = -f_{2L} K_B^2 \omega_p^2 \omega_0 \gamma^{-5} \times a_w^2 (t/2)^3 h$	$\pi / k_w L$
High gain strong pump regime $\beta_\perp \gg \beta_{\text{crit}}$	$\frac{\sqrt{3}}{2^{5/3}\gamma} (f_2 K_B^2 \omega_p^2 \omega_0 a_w^2)^{1/3}$	$\frac{\gamma}{2^{2/3}} \left(f_2 K_B^2 \frac{\omega_p^2}{\omega_0^2} a_w^2 \right)^{1/3}$	$\frac{\sqrt{3}}{2^{5/3}\gamma\gamma_\parallel^{2/3}} (f_{2L} K_B^2 \omega_p^2 \omega_0 a_w^2)^{1/3}$	$\frac{\gamma_\parallel^{4/3}\gamma^{-1}}{2^{2/3}} \left(f_{2L} K_B^2 \frac{\omega_p^2}{\omega_0^2} a_w^2 \right)^{1/3}$
High gain weak pump, Raman regime $\beta_\perp \ll \beta_{\text{crit}}$	Negative mass instability $\simeq f^{1/2} \frac{\omega_p}{\gamma^{1/2}}$	...	$(1/2^{3/2})(f_{2L}^{1/2}/f_{1L}^{1/4}) \times (\omega_p \omega_0 K_B^2 a_w^2 / \gamma_\parallel \gamma^{5/2})^{1/2}$	$2 f_{1L}^{1/2} \frac{\gamma_\parallel}{\gamma^{1/2}} \frac{\omega_p}{\omega_0}$

$h = h(\Delta\omega t/2) = \frac{d}{dx}\left(\frac{\sin x}{x}\right)^2\Big|_{x=\Delta\omega t/2}$, $\gamma_\parallel = \gamma/(1+a_w^2)^{1/2}$, L = total length of wiggler field,

$\beta_{\text{crit}} = (2^{5/2}/3^{3/4})(f_1^3/f_2^2 K_B^4)^{1/4} \gamma^{-1/4} (\omega_p/\omega_0)^{1/2}$, $\beta_{\text{crit},L} = (2^{5/2}/3^{3/4})(f_{1L}^3/f_{2L}^2 K_B^4)^{1/4} (\gamma_\parallel^2 \gamma)^{-1/4} (\omega_p/\omega_0)^{1/2}$,

$K_B = J_0(R) - J_1(R)$, $R = a_w^2/2(1+a_w^2)$.

See Sec. II for f_1 and f_2.

IV. HIGH GAIN REGIME

A. Dispersion equation

This section examines the high gain regime, in which the radiation field undergoes exponential growth. The complex representation, in which $a_s(t) = |a_s(t)| e^{i\phi_s(t)}$, is used. Energy spread and space charge are examined in this section.

We begin the linearization of Eqs. (17), (19), and (23) by defining the perturbed quantities $\delta\gamma_j$, $\delta\zeta_j$, and δa_s:

$$\zeta_j = \zeta_{j0} + \Delta\omega_j t + \delta\zeta_j, \quad \gamma_j = \gamma_{j0} + \delta\gamma_j, \quad a_s = \delta a_s, \tag{44}$$

where the subscript "$j0$" refers to the initial values of the jth electron. The frequency detuning for the jth electron is

$$\Delta\omega_j = (p+N)(\omega_c/\gamma_{j0})(1 - a_w^2/2\gamma_{j0}^2) - \omega_s. \tag{45}$$

The time dependence of the perturbations is given as

$$\begin{aligned} \delta\zeta_j &= \tfrac{1}{2}\{\delta\tilde{\zeta}_j \exp[i(\zeta_{j0} + \Delta\omega_j t + \Gamma t)] + \text{c.c.}\}, \\ \delta\gamma_j &= \tfrac{1}{2}\{\delta\tilde{\gamma}_j \exp[i(\zeta_{j0} + \Delta\omega_j t + \Gamma t)] + \text{c.c.}\}, \\ \delta a_s &= \delta\tilde{a}_s \exp(i\Gamma t), \end{aligned} \tag{46}$$

where $-\operatorname{Im}\Gamma$ is the growth rate ω_i of the radiation mode.

Substituting Eqs. (44) and (46) in Eqs. (17), (19), and (23) yields the linearized equations for $\delta\zeta_j$, $\delta\gamma_j$, and δa_s:

$$\begin{aligned} &\tfrac{1}{2}\{i(\Delta\omega_j + \Gamma)\delta\tilde{\zeta}_j \exp[i(\zeta_{j0} + \Delta\omega_j t + \Gamma t)] + \text{c.c.}\} \\ &\quad = \frac{1}{2}\left[-(p+N)\frac{\omega_c}{\gamma_{j0}^2}\left(1 - \frac{3a_w^2}{2\gamma_{j0}^2}\right)\right] \\ &\qquad \times\{\delta\tilde{\gamma}_j \exp[i(\zeta_{j0} + \Delta\omega_j t + \Gamma t)] + \text{c.c.}\} \\ &\qquad + \frac{1}{2}\left((p+N)\frac{\omega_c}{\gamma_{j0}^3} K_B a_w \right. \\ &\qquad \left. \times \exp[i(\zeta_{j0} + \Delta\omega_j t + \Gamma t)]\delta\tilde{a}_s + \text{c.c.}\right), \\ &\tfrac{1}{2}\{i(\Delta\omega_j + \Gamma)\delta\tilde{\gamma}_j \exp[i(\zeta_{j0} + \Delta\omega_j t + \Gamma t)] + \text{c.c.}\} \\ &\quad = \frac{1}{2}\left(i\omega_s K_B a_w \frac{1}{\gamma_{j0}} \right. \\ &\qquad \left. \times \exp[i(\zeta_{j0} + \Delta\omega_j t + \Gamma t)]\delta\tilde{a}_s + \text{c.c.}\right) \\ &\qquad - \frac{1}{2}\frac{f_1\omega_p^2}{(p+N)\omega_c/\gamma_{j0}} \\ &\qquad \times\{\langle\delta\tilde{\zeta}_j\rangle \exp[i(\zeta_{j0} + \Delta\omega_j t + \Gamma t)] + \text{c.c.}\}, \end{aligned} \tag{47}$$

$$\Gamma\delta\tilde{a}_s = -f_2 \frac{\omega_p^2 K_B a_w}{4\omega_s}\left\langle \frac{\delta\tilde{\gamma}_j}{\gamma_{j0}^2} + i\frac{\delta\tilde{\zeta}_j}{\gamma_{j0}} \right\rangle.$$

An initial distribution that is independent of the electron phase ζ was assumed. Using the k and k_w defined in Sec. II C, Eqs. (47) of the circular FEL become identical to the similar small signal equations of the linear FEL, except for the underlined coefficient of $\delta\tilde{\gamma}_j$. This coefficient is the factor Q defined in Sec. III.

A straightforward algebraic calculation yields the dispersion equation from Eq. (47):

$$\begin{aligned} 1 = &-\frac{f_2\omega_p^2 K_B^2 a_w^2}{4\Gamma}\left\{ \alpha_3 + \frac{(p+N)\omega_c}{\omega_s} \right. \\ &\times\left[\alpha_4 - \omega_s\left(\beta_4 - \frac{3}{2}a_w^2\beta_6\right)\right] \\ &+ \frac{f_1\omega_p^2}{(1+\chi_\parallel)\omega_s}\left[\alpha_1 - (p+N)\omega_c\left(\beta_2 - \frac{3}{2}a_w^2\beta_4\right)\right] \\ &\left.\times\left[\alpha_3 - \omega_s\left(\beta_3 - \frac{3}{2}a_w^2\beta_5\right)\right]\right\}, \end{aligned} \tag{48}$$

where

$$\alpha_n = \langle(\Delta\omega_j + \Gamma)^{-1}\gamma_{j0}^{-n}\rangle, \quad \beta_n = \langle(\Delta\omega_j + \Gamma)^{-2}\gamma_{j0}^{-n}\rangle, \tag{49}$$

and $\chi_\parallel$ denotes the electron susceptibility defined by

$$\chi_\parallel = f_1\omega_p^2[\beta_1 - (3a_w^2/2)\beta_3]. \tag{50}$$

The susceptibility $\chi_{\parallel}$ is proportional to Q. Note that the electron susceptibility $\chi_{\parallel}$ of the circular FEL is positive, while the space-charge wave in the linear FEL geometry has a negative susceptibility,

$$\chi_{\parallel} = -f_{1L}\omega_p^2\beta_3(1+a_w^2) \quad \text{(linear FEL)}. \tag{51}$$

This difference is a consequence of the negative mass effect in the circular FEL, where the electrons are subject to the cyclotron motion slightly perturbed by the wiggler field.

Next we introduce energy spread. The unperturbed distribution function is assumed to be uniform in the range of $|\gamma-\gamma_0|<\Delta\gamma$, where the energy spread is small, $\Delta\gamma/\gamma_0 \ll 1$. For $\Delta\gamma/\gamma_0 \ll 1$, the frequency detuning Eq. (45) for the jth electron in the circular FEL is given approximately by

$$\Delta\omega_j \simeq \Delta\omega_0 - \omega_0(\Delta\gamma_j/\gamma_0), \tag{52}$$

where $\Delta\gamma_j = \gamma_j - \gamma_0$, $\Delta\omega_0 = \omega_0 - \omega_s$, and ω_0 is defined in Eq. (18). For comparison, the linear FEL has the frequency detuning

$$\Delta\omega_j \simeq \Delta\omega_0 + \omega_0(\Delta\gamma_j/\gamma_0^3) \quad \text{(linear FEL)}, \tag{53}$$

where ω_0 is defined by Eq. (29) and $\Delta\omega_0 = \omega_0 - \omega_s$. We note that the frequency detuning $\Delta\omega_j$ of the circular FEL is more sensitive to the energy spread than that of the linear FEL by a factor of γ_0^2. This results in a greater sensitivity of the growth rate to the energy spread in the circular FEL, as shown in Sec. IV C.

The full dispersion relation is found using

$$\beta_n = \gamma_0^{-n}[\Gamma^2 + 2\Delta\omega_0\Gamma + \Delta\omega_0^2 - (\omega_0\Delta\gamma/\gamma_0)^2]^{-1}, \tag{54}$$

which, together with α_n, appears in Eq. (48). However, the ratio of the two terms is an order of $\Delta\omega_0/\omega_s$, and we can neglect α_n.

With these approximations, the cubic dispersion equation of the circular FEL can be obtained using Eqs. (48) and (54):

$$\Gamma^3 + 2\Delta\omega_0\Gamma^2 + \left[\Delta\omega_0^2 - \left(\omega_0\frac{\Delta\gamma}{\gamma_0}\right)^2 + \frac{f_1\omega_p^2}{\gamma_0}\left(1-\frac{3a_w^2}{2\gamma_0^2}\right)\right]\Gamma = \frac{f_2\omega_p^2\omega_0 K_B^2 a_w^2}{4\gamma_0^3}. \tag{55}$$

B. Comparison with the linear FEL

To understand the dispersion relation of the circular FEL, it is useful to recall the dispersion equation of the linear FEL with no guiding axial magnetic field[9,10]:

$$\Gamma^3 + 2\Delta\omega_0\Gamma^2 + \left[\Delta\omega_0^2 - \left(\omega_0\frac{\Delta\gamma}{\gamma_0^3}\right)^2 - \frac{f_{1L}\omega_p^2}{\gamma_0^3}(1+a_w^2)\right]\Gamma = -\frac{f_{2L}\omega_p^2\omega_0 K_B^2 a_w^2}{4\gamma_0^5}(1+a_w^2). \tag{56}$$

The dispersion relations (55) and (56), for the circular FEL and the linear FEL, have three terms that differ. First, from the factor Q defined in Eq. (39), the coupling terms (the right-hand side) differ by $-\gamma_0^2$. This increases the growth rate and the efficiency of the circular FEL as shown in Sec. IV C. Second, the space-charge terms differ by $-\gamma_0^2$. This term corresponds to the electron susceptibility in Eqs. (50) and (51). The positive susceptibility of the circular FEL causes the negative mass instability. The third difference is in the energy-spread term in the linear coefficient of Γ. The circular FEL is more sensitive to the energy spread than is the linear FEL, as shown in Sec. IV D.

The circular FEL is characterized by the coupling between the positive energy electromagnetic wave and the negative energy space-charge wave, which is itself unstable because of the negative mass effect. By comparison, the conventional linear FEL couples the electromagnetic wave with the stable beam space-charge mode. Setting $a_w = 0$ in the equations for the circular FEL, Eqs. (17), (19), and (23), the radiation field terms disappear and the equations describe only the space-charge wave in the θ direction. The frequency $\Gamma + \Delta\omega_0$ of these space-charge waves can be obtained by setting $a_w = 0$ in Eqs. (55) and (56):

$$\Gamma + \Delta\omega_0 = \begin{cases} \pm i f_1^{1/2}(\omega_p/\gamma_0^{1/2}) & \text{(circular FEL)}, \\ \pm f_{1L}^{1/2}(\omega_p/\gamma_0^{3/2}) & \text{(linear FEL)}, \end{cases} \tag{57}$$

where a cold beam approximation, $\Delta\gamma = 0$, has been made. The stabilization of the negative mass instability by the waveguide wall or by energy spread is discussed in Appendix A.

The linear FEL with an axial magnetic field is another case in which the FEL instability can couple with an unstable space-charge wave. The space-charge wave is driven unstable by the presence of the wiggler and the axial magnetic field in a particular parameter region.[16,17] As is the case here, the FEL instability is enhanced by the presence of an unstable space-charge wave.

C. Cold beam limit

The dispersion relation of the circular FEL in the cold beam, strong pump limit is obtained by neglecting the space-charge wave and setting $\Delta\gamma = 0$ in Eq. (55):

$$\Gamma^3 + 2\Delta\omega_0\Gamma^2 + \Delta\omega_0^2\Gamma = f_2\omega_p^2\omega_0 K_B^2 a_w^2/4\gamma_0^3. \tag{58}$$

The peak growth rate of the strong pump regime of the circular FEL occurs for $\Delta\omega_0 = 0$:

$$\omega_i = (\sqrt{3}/2^{5/3}\gamma_0)(f_2\omega_p^2\omega_0 K_B^2 a_w^2)^{1/3}. \tag{59}$$

The efficiency η is easily obtained by using well-known techniques[18]:

$$\eta = (\gamma_0/2^{2/3})[f_2(\omega_p^2/\omega_0^2)K_B^2 a_w^2]^{1/3}. \tag{60}$$

Table I contains the growth rates and efficiencies for the circular and linear FEL. In the strong pump, cold beam parameter region, the growth rate and the efficiency of the circular FEL are larger than those of the linear FEL by a factor of $\gamma_0^{2/3}$.

The circular and linear geometries behave quite differently in the weak pump (Raman) regime. In the linear FEL the weak pump regime begins when

$$\beta_\perp = \frac{a_w}{\gamma_0} < \beta_{\text{crit},L} = \frac{2^{5/2}}{3^{3/4}}\left(\frac{f_{1L}^3}{f_{2L}^2 K_B^4}\right)^{1/4}(\gamma_0\gamma_\parallel^2)^{-1/4}\left(\frac{\omega_p}{\omega_0}\right)^{1/2}, \tag{61}$$

where $\gamma_{\parallel} = \gamma_0/(1 + a_w^2)^{1/2}$.

In the circular FEL, however, the susceptibility [Eq. (50)] is positive and the term proportional to $\omega_p^2\Gamma$ in Eq. (55) corresponds to an instability. Thus, instead of the FEL instability, the negative mass instability dominates in the weak pump regime of the circular FEL. Its growth rate is found, from Eq. (57), to be

$$\omega_i = f_1^{1/2}\,(\omega_p/\gamma_0^{1/2}) \quad \text{(negative mass instability)}. \tag{62}$$

This result agrees with the well-known growth rate of the negative mass instability[14] (see Appendix A). The condition for the circular FEL to be in the strong pump regime is that the growth rate [Eq. (59)] of the FEL is much larger than that [Eq. (62)] of the negative mass instability. This corresponds to requiring that $\beta_\perp \gg \beta_{\text{crit}}$ for the strong pump regime of the circular FEL, where

$$\beta_{\text{crit}} = \frac{2^{5/2}}{3^{3/4}}\left(\frac{f_1^3}{K_B^4 f_2^2}\right)^{1/4}\gamma_0^{-1/4}\left(\frac{\omega_p}{\omega_0}\right)^{1/2}. \tag{63}$$

We summarize the above results in Table I.

In Figs. 2 and 3, the cold beam growth rate of the circular [Eq. (55)] and linear [Eq. (56)] FEL are solved for numerically. The normalized growth rate ω_i/ω_0 as a function of the normalized detuning parameter $\Delta\omega_0/\omega_0$, is plotted for the circular FEL in Fig. 2 and the linear FEL in Fig. 3. For both Figs. 2 and 3, $\gamma_0 = 5$, $a_w = 2$, and the plasma frequency varies. For the sake of simplicity, we assume $f_1 = f_{1L} = 1$ for the cases plotted with solid lines in Figs. 2 and 3.

In the circular FEL, the instability near the peak $\Delta\omega_0 \simeq 0$ is mostly a strong pump FEL interaction, which agrees with the analytic expression of the growth rate [Eq. (59)]. These peak growth rates are larger than those of the linear FEL by about $\simeq\gamma_0^{2/3}$. As the frequency detunes, the character of the instability becomes increasingly electrostatic. This negative mass instability is very wideband and its asymptotic growth rate is independent of wiggler field strength [Eq. (62)]. As the plasma frequency increases, the negative mass instability becomes more dominant because of the increase in β_{crit} defined in Eq. (63). To show the effect of the negative mass instability explicitly, we set $f_1 = 0$ for the case plotted by the broken line in Fig. 2 ($\omega_p/\omega_0 = 2\times10^{-2}$). With $f_1 = 0$ the bandwidth of the FEL instability becomes narrow and the peak growth rate decreases.

In Fig. 4 we plot the peak growth rate of both FEL's as functions of the pump field strength $\beta_\perp$, for the case of $\gamma_0 = 5, \omega_p/\omega_0 = 2\times10^{-2}$, and 5×10^{-3}. In the strong pump regime, the circular FEL has the larger growth rate, with the same scaling $\beta_\perp^{2/3}$ as that of the linear FEL. However, in the weak pump regime, the negative mass instability dominates and the growth rate is independent of the pump field strength $\beta_\perp$.

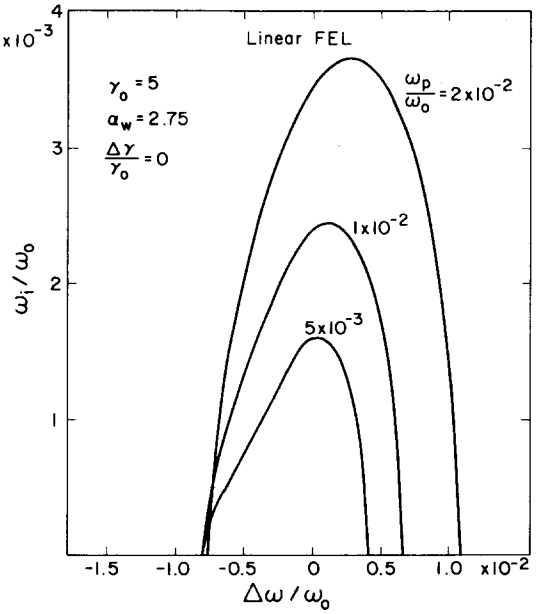

FIG. 3. The growth rate ω_i/ω_0 of the linear FEL as a function of detuning $\Delta\omega_0/\omega_0$. The parameters are the same as those of Fig. 2.

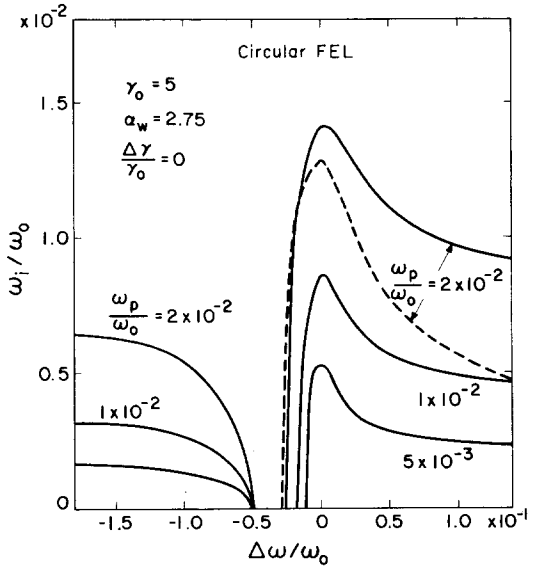

FIG. 2. The growth rate ω_i/ω_0 of the circular FEL as a function of detuning $\Delta\omega_0/\omega_0$, for $\gamma_0 = 5$, $a_w = 2.75$, $\Delta\gamma/\gamma_0 = 0$, $f_2 = 1$, and a varying plasma frequency. Here $f_1 = 1$ for the solid lines. In the broken line, the space-charge effect is neglected ($f_1 = 0$).

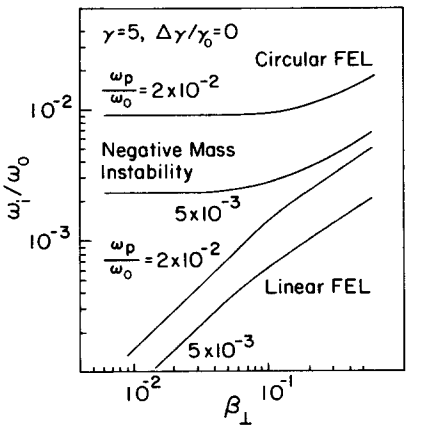

FIG. 4. The growth rate ω_i/ω_0 as a function of the pump field strength $\beta_\perp$. The parameters are $\gamma_0 = 5$, $\Delta\gamma/\gamma_0 = 0$, $f_1 = f_2 = 1$, $\omega_p/\omega_0 = 2\times10^{-2}$ and 5×10^{-3}.

D. Energy spread

The effect of energy spread is examined by numerically solving the cubic dispersion equations (55) and (56). The normalized growth rates ω_i/ω_0 from the dispersion equations (55) and (56) are shown as functions of the normalized detuning parameter $\Delta\omega_0/\omega_0$ for the circular FEL (Fig. 5) and the linear FEL (Fig. 6), with $\gamma_0 = 5$, $a_w = 2$, $\omega_p/\omega_0 = 2\times 10^{-2}$, and varying values of the energy spread $\Delta\gamma/\gamma_0$. The growth rate of the circular FEL starts decreasing at a smaller energy spread than would the linear FEL. The negative mass contribution to the growth rate is effectively suppressed by the energy spread.

Figure 7 shows the normalized growth rate ω_i/ω_0 as a function of the energy spread $\Delta\gamma/\gamma_0$ for circular and linear FEL's, with $\gamma_0 = 5$, $a_w = 2$, and varying values of the plasma frequency. The growth rate of the circular FEL starts degrading at a smaller energy spread than would the linear FEL. This critical value of the velocity spread increases with increasing plasma frequency. As the energy spread begins to substantially reduce the gain, the square distribution function used to derive the cubic dispersion relations (55) and (56) should be replaced by a more realistic model.

If the electrons have an energy spread $\Delta\gamma$, the electron beam has a nonzero beam width Δr. Equation (11) gives the simple relation between $\Delta\gamma$ and Δr:

$$\Delta r/r_0 = \Delta\gamma/\gamma_0, \tag{64}$$

where $\beta_0 \simeq 1$ is assumed. Note that Δr and $\Delta\gamma$ are defined as the half-width.

The energy spread not only affects the gain through the linear term in the cubic dispersion relation, but also through the beam–mode overlap. As will be shown in Sec. V A, optimum coupling requires maximization of the spatial overlap factor f_2 by adjusting the electron-beam position r_0. For a beam with zero radial width, the optimal coupling occurs when the electron-beam radius is located at the peak of the mode profile. With a beam of nonzero width, the coupling factor f_2 is reduced. Using the definition of f_2 [Eq. (24)], and Taylor expanding Bessel functions in $\Delta r/r_0$, we find $\Delta f_2/f_2 \simeq p^2(\Delta r/r_0)^2$. Here Δf_2 is the reduction in coupling for a beam at radius $r = r_0 + \Delta r$. Equation (64) can then be used to obtain the desired criterion on the energy spread:

$$\Delta\gamma/\gamma_0 \ll 1/p. \tag{65}$$

This condition implies that TM_{pq} modes with high p (or high frequency) can be coupled to efficiently by a beam with a small energy spread. For example, we need $\Delta\gamma/\gamma_0 \ll 10^{-2}$ to couple effectively to a TM_{pq} mode with $p = 100$.

Another constraint on the energy spread is given by the azimuthal component of the wiggler field. The full wiggler field is given by Eq. (1) and includes an azimuthal component. By choosing the radii a' and b' of the outer and inner magnets, such that $r_0 = (a'^{N-1}b'^{N+1})^{1/2N}$, the azimuthal component vanishes at the electron-beam position r_0. However, the azimuthal component exists at radii other than $r = r_0$. This field component, as well as gradients in the radial field, influence the orbits of electrons with $r \neq r_0$. While the detailed orbit calculations are left for future investigations, a

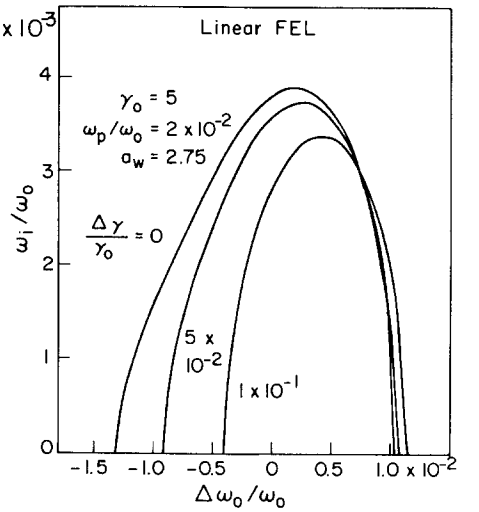

FIG. 6. The growth rate ω_i/ω_0 of the linear FEL as a function of detuning $\Delta\omega_0/\omega_0$. The parameters are the same as those of Fig. 5.

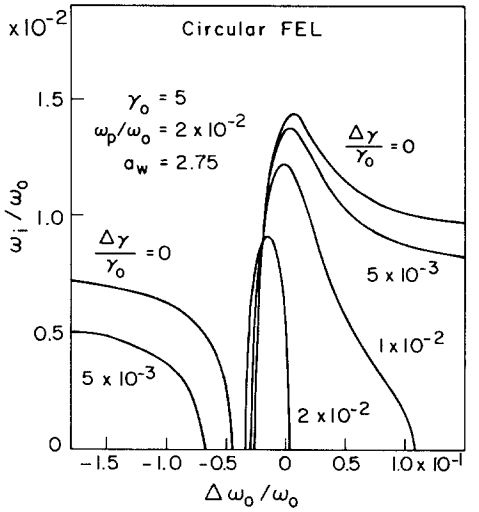

FIG. 5. The growth rate ω_i/ω_0 of the circular FEL as a function of detuning $\Delta\omega_0/\omega_0$, for $\gamma_0 = 5$, $\omega_p/\omega_0 = 2\times 10^{-2}$, $a_w = 2.75$, $f_1 = 1$, and a varying energy spread.

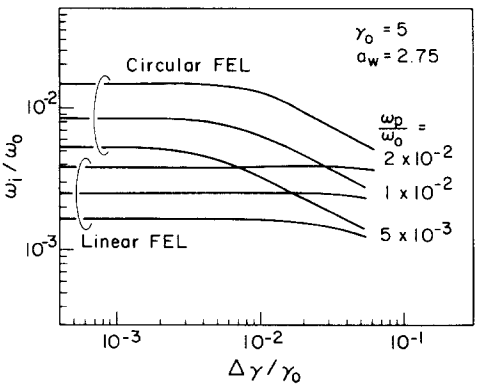

FIG. 7. The growth rate ω_i/ω_0 as a function of the energy spread. The parameters are $\Delta\gamma_0/\gamma_0$ for $\gamma_0 = 5$, $a_w = 2.75$, $f_1 = f_2 = 1$, and a varying plasma frequency.

criterion similar to $k_w r_e \ll 1$ for the linear FEL can be derived. Let $\tilde{B}_{w\theta}$ and $\tilde{B}_{wr}$ be spatial amplitudes of the azimuthal and the radial components of the wiggler. Using Eq. (1), we find $\tilde{B}_{w\theta}/\tilde{B}_{wr} \simeq N(\Delta r/r_0)$. Thus neglecting the azimuthal field component requires

$$\Delta\gamma/\gamma_0 \ll 1/N. \tag{66}$$

Since $N \ll p$, the spatial coupling criterion equation (65) is more difficult to satisfy than the criterion equation (66) for the one-dimensional approximation of the wiggler field.

V. DISCUSSION

A. Optimization of beam position

To optimize the gain of a given mode, it is necessary to maximize the spatial coupling factor f_2 by choosing of the electron-beam position. As is seen in Eq. (24), f_2 is proportional to the square of the electronic field amplitude at the beam radius.

Even if the beam is optimized for coupling to one specific mode, other nearby modes may also be amplified. Using Eq. (34) for a low-aspect-ratio waveguide $(a-b)/a \ll 1$, the azimuthal mode number of the radiation with radial mode number q is given by

$$p_{\pm} = [1/(\sigma_+^2 - 1)] \times \{N \pm [N^2\sigma_+^2 - q^2\sigma_-^2(\sigma_+^2 - 1)]^{1/2}\}, \tag{67}$$

where $\sigma_+ = \omega_+/(\omega_c\gamma_0^{-1})$, $\sigma_- = \omega_-/(\omega_c\gamma_0^{-1})$, $\omega_+ = 2c/(a+b)$, $\omega_- = \pi c/(a-b)$, and we assume that $\sigma_-^2 \gg \sigma_+^2$. These two solutions correspond to the high- and low-frequency branches of the FEL instability. Negative values of p correspond to modes traveling in the $-\theta$ direction.

The number of modes that can couple varies according to whether $\sigma_+ \lesssim 1$. It is found from Eq. (11) that $\sigma_+ \lesssim 1$ occurs when the electron-beam position $r_0 \lesssim \beta_0(a+b)/2$. If $\sigma_+ > 1$, then only a finite number of radial modes with $(1 \leqslant q \leqslant q_h)$ have two solutions $p_+(q)$ and $p_-(q)$; here $q_h = N(\sigma_+/\sigma_-)(\sigma_+^2 - 1)^{-1/2}$. For $\sigma_+ < 1$, an infinite number of radial modes ($q = 1,2,\ldots$) have two solutions $p_+(q)$, $p_-(q)$. To avoid possible multimode oscillations, the number of possible modes that may oscillate should be reduced. This can be achieved by putting the electron beam in the outer half of the gap $[r_0 > \beta_0(a+b)/2]$ and decreasing q_h.

In most cases of interest, the radiation field has an azimuthal index $p \gg 1$. Higher-order azimuthal modes of coaxial waveguides are characterized by whispering-gallery modes, in which the field energy is localized near the outer electrode. The location of the peak of the field shifts outward as p increases. Figure 8 illustrates this. The solid lines of Fig. 8 show the position r_p (the left vertical axis) of the peak amplitude of the electric field of the TM_{pq} mode for $q = 1$ as a function of p, for a coaxial waveguide with $a = 6.51$ cm, $b = 5.40$ cm. The broken lines are the possible oscillating mode numbers p_+, p_- for $\gamma_0 = 5.1$, $N = 12$, and $q = 1$ as a function of the axial magnetic field B_0 (the right vertical axis). The axial magnetic field also determines the electron-cyclotron radius r_0. The intersection of the solid line (the position of the peak amplitude of the TM_{pq} mode) and the broken line (the electron-beam radius) gives the optimum

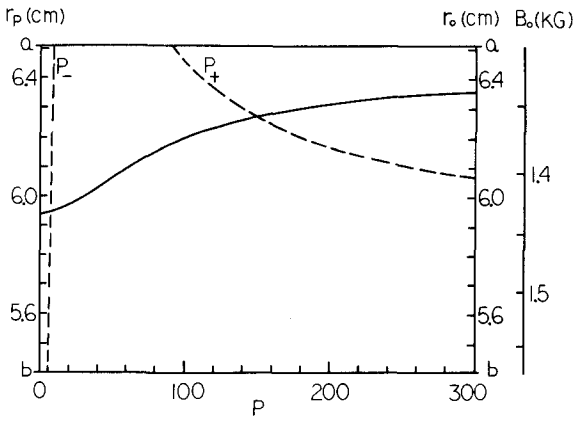

FIG. 8. The diameter for the spatial coupling optimization. The solid lines are positions r_p for the peak field of the TM_{pq} modes as functions of p for $q = 1$. The broken lines are p_-, p_+, the azimuthal mode numbers, as functions of the axial magnetic field B_0 or electron-beam radius r_0 for $N = 12$, $q = 1$, $\gamma_0 = 5.1$, $a = 6.51$ cm, $b = 5.40$ cm.

condition (B_0 or r_0) for the maximum coupling between the field and the electron beam.

Figure 9 shows the result of the optimizing for each radial mode by adjusting the axial magnetic field. The frequency [Fig. 9(a)] and the growth rate [Fig. 9(b)] are shown for $\gamma_0 = 5.1$, $\Delta\gamma = 0$, $N = 12$, $a = 6.51$ cm, $b = 5.40$ cm, $\omega_p = 1.78 \times 10^{10}$ sec^{-1}, and $\tilde{B}_w = 6.72$ kG as functions of the axial magnetic field or the electron-beam radius. The growth rate is calculated from Eq. (59), neglecting the negative mass instability. The solid and the broken lines are, respectively, the high- and low-frequency branches. The region $r_0 < \beta_0(a+b)/2 = 5.84$ cm corresponds to $\sigma_+ < 1$, and there are an infinite number of possible modes with different radial mode numbers q. The higher modes $q \geqslant 5$ are omitted from Fig. 9 for the sake of simplicity. The region $r_0 > 5.84$ cm corresponds to $\sigma_+ > 1$, and there are a finite number of modes with $q \leqslant q_h$. When the electron beam is near the midpoint of the gap, the mode number of the high-frequency branch rapidly increases. The high p values place constraints on beam energy spread, which seem difficult to satisfy (see Sec. IV D); therefore the growth rate of such modes is not plotted in Fig. 9(b). These modes occur for radii between 5.76 cm and 5.90 cm. While the axial magnetic field varies from 1.35 to 1.45 kG, each of the modes with $q = 1,2,3$, and 4 has a maximum growth rate at the optimum point for each mode. These optimum parameters can be obtained by means of the optimizing scheme in Fig. 8. The peak of the higher radial mode corresponds to the high p number.

B. Bandwidth

Schuetz and co-workers[19] pointed out that the circular FEL can be used as a wideband amplifier. In this section we evaluate the bandwidth of the circular FEL and find a similar result.

As the radiation frequency ω_s departs from the center frequency ω_0, $\Delta\omega_0$ become finite. Solving the dispersion

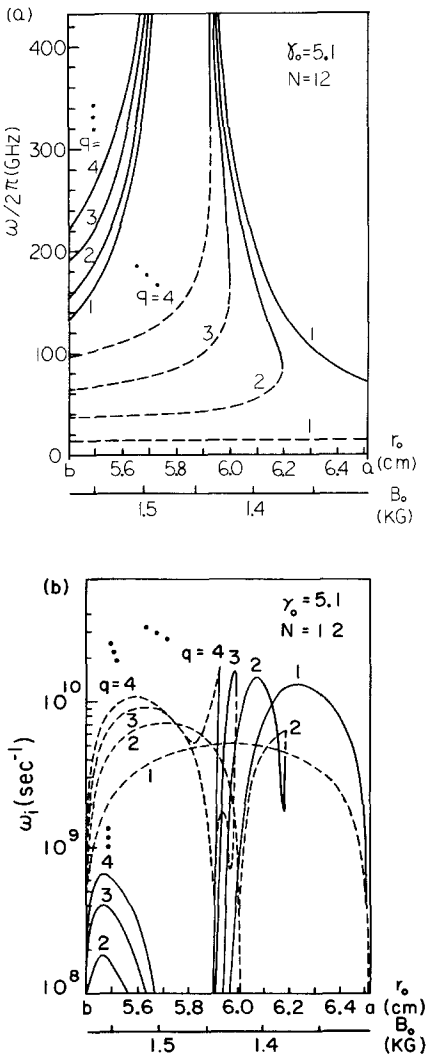

FIG. 9. Example of gain optimization by adjusting axial magnetic field: (a) frequency $\omega/2\pi$ and (b) growth rate ω_i as a function of axial magnetic field B_0 or electron-beam radius r_0. The solid and broken lines correspond to the high-frequency and low-frequency branches of the interaction, respectively. Higher modes $q \geqslant 5$ are omitted from the figures. The parameters are $N = 12$, $\gamma_0 = 5.1$, $\omega_p = 1.78 \times 10^{10}\ \mathrm{sec}^{-1}$, $\tilde{B}_w = 6.72$ kG, $a = 6.51$ cm, and $b = 5.40$ cm.

equation (55), a typical width $\Delta\omega_0$ of the detuning can be estimated. The corresponding radiation-frequency width $\delta\omega_s$ depends on the slopes of the dispersion curve of the waveguide and the beam mode. Using Eq. (18) and the dispersion relation of the waveguide, we find the radiation-frequency width:

$$\delta\omega_s = \Delta\omega_0 \left[\frac{\omega_c}{\gamma} \left(\frac{d\omega_s}{dp} \right)^{-1} - 1 \right]^{-1} \tag{68}$$

where $d\omega_s/dp$ is the derivative of the waveguide frequency with respect to p. If $(a-b)/a \ll 1$, differentiation of Eq. (34) yields $d\omega_s/dp = (\omega_+^2/\omega_s)p$. The coaxial waveguide size (or ω_+), the axial magnetic field, and the electron energy can be chosen such that $d\omega_s/dp \approx \omega_c/\gamma_0$. This choice means that the two dispersion curves are grazing. Note that this grazing condition is identical to $\sigma_+ = 1$ for a coaxial waveguide with a small gap, where σ_+ is defined in Sec. V A. The circular FEL frequency spectrum may be very wideband when the dispersion curves are grazing.

Another factor that determines the bandwidth is the spatial coupling between the electron beam and the radiation field. As Fig. 8 shows, the peak position of the TM_{pq} mode shifts outward as p increases. The typical radial width of the TM_{pq} mode is roughly $\sim r_0/p$ $(p \gg 1)$ (see Sec. IV D). Assuming that the peak position of the TM_{pq} mode coincides with the electron-beam position r_0, modes from TM_{pq} to $TM_{p+\delta p,q}$ may couple efficiently with the electron beam. The peak position of the $TM_{p+\delta p,q}$ mode is at $r_0 + r_0/p$. This δp is approximately given by

$$\delta p \approx \frac{r_0}{p} \left(\frac{dr_p}{dp} \right)^{-1}, \tag{69}$$

where r_p is the location of the radial maximum of the TM_{pq} mode. As an example, we can evaluate dr_p/dp of the coaxial waveguide of Fig. 9, using Fig. 8. The corresponding bandwidth is given by $\delta\omega_s = (d\omega_s/dp)\delta p$.

In summary, two factors that limit the bandwidth are the dispersion and the spatial coupling. As a typical value, we find $\delta\omega_s/\omega_s \approx 0.3$ for the parameters of Fig. 9, with $B_0 = 1.4$ kG, $q = 2$. This shows that the circular FEL may work as a wideband amplifier.

VI. CONCLUSIONS

We have examined the linear theory of the circular FEL in a one-dimensional model. This model includes longitudinal space charge, transverse coaxial waveguide modes, and energy spread. Linearization of the equations of motion yields a cubic dispersion relation.

We study this cubic dispersion relation for the circular FEL and compare it with that of the linear FEL. Analytic expressions for the gain in the low gain regime and the growth rate in the strong pump and negative mass dominated regimes are derived. These results are summarized in Table I. The coupling term between the space-charge wave and electromagnetic mode is found to be larger for the circular FEL by a factor of γ^2. The circular FEL, however, is more sensitive to energy spread than the linear FEL.

Another new result found here is the influence of the negative mass instability on the FEL growth rate. Unlike the linear FEL, the circular FEL does not have a weak pump (Raman) regime. Instead, the FEL growth rate becomes identical to that of the unstable space-charge wave. In the strong pump regime, the FEL peak growth rate is enhanced by the negative mass instability and the bandwidth is increased.

ACKNOWLEDGMENTS

We wish to thank George Bekefi, Ronald Davidson, and Han Uhm for useful discussions.

This work was supported in part (H.S.) by the Japan Society for the Promotion of Science and in part (J.W.) by the Office of Naval Research.

APPENDIX: DERIVATION OF f_1 IN EQ. (21)

The negative mass instability has been studied by many authors.[12–15] Uhm and Davidson[14] analyzed the negative mass instability of an intense relativistic electron beam utilizing a kinetic description that includes the equilibrium self-field, the transverse magnetic perturbations, the inner and outer cylindrical conductor, and the spread in canonical angular momentum (ΔP). The growth rate ω_i is given in Eq. (92) of Ref. 14 assuming

$$1 \leqslant l \ll r_0/\Delta r, \tag{A1}$$

where l is the azimuthal harmonic number and $l = p + N$ for the negative mass instability in the circular FEL. The condition (A1) is equivalent to the spatial coupling criterion [Eq. (65)] in the text. Therefore (A1) should be satisfied in the circular FEL. The spread in canonical angular momentum (Δ) in Ref. 14 can be written as $\Delta P = mcr_0\Delta\gamma$, where $\Delta\gamma$ is also the energy spread in our notation. The growth rate of Eq. (92) in Ref. 14 is expressed in our notation as

$$\omega_i^2 = lg\frac{a^2 - b^2}{4r_0^2}\frac{\omega_p^2}{\gamma_0} - \left(\omega_0\frac{\Delta\gamma}{\gamma_0}\right)^2. \tag{A2}$$

The second term of Eq. (A2) shows the stabilizing influence of beam energy spread. The first term is geometric and g is defined in Eq. (22) of the text. The quantities $b_\pm$ in Eq. (22) are the wave admittances at the inner and outer boundaries of the electron beam and are given by

$$b_+ = -i(E_r/E_\theta)|_{r=r_0+\Delta r}, \tag{A3}$$

$$b_- = i(E_r/E_\theta)|_{r=r_0-\Delta r}, \tag{A4}$$

where $r_0 \pm \Delta r$ are the radii of the inner and outer boundaries of the beam. For the coaxial waveguide, $b_\pm$ are

$$b_+ = -\frac{lc}{r_0\omega_s}\frac{Y_l'(k_r a)J_l(k_r r_0) - J_l'(k_r a)Y_l(k_r r_0)}{Y_l'(k_r a)J_l'(k_r r_0) - J_l'(k_r a)Y_l'(k_r r_0)}, \tag{A5}$$

$$b_- = \frac{lc}{r_0\omega_s}\frac{Y_l'(k_r b)J_l(k_r r_0) - J_l'(k_r b)Y_l(k_r r_0)}{Y_l'(k_r b)J_l'(k_r r_0) - J_l'(k_r b)Y_l'(k_r r_0)}. \tag{A6}$$

In Fig. 10 we plot $(b_+ + b_-)/2$ for the parameters of Fig. 9 ($a = 6.51$ cm, $b = 5.40$ cm, $\gamma_0 = 5.1$), and varying electron beam radii. Note that $lc/r_0\omega_s$ in Eqs. (A5) and (A6) reduces to l/β_0 and b_+, b_- are functions of l, γ_0, a/r_0, and b/r_0. The negative mass instability has a significant impact on the peak value and the spectrum shape of the growth rate in the circular FEL, as is shown in Sec. IV C. The growth rate of the negative mass instability depends on f_1 and it is stabilized when $f_1 < 0$. When the width of the electron beam is not too large [see Eq. (22)], the wave admittance alone determines the value (and sign) of f_1. Generally, $(b_+ + b_-)/2$ oscillates from the negative to the positive value with an almost constant period of l and gradually tends to γ_0. An inductive impedance at the beam corresponds to $b_+ + b_- < 0$ and the negative mass instability is then stabilized by the waveguide. In the case of an inductive impedance, the stabilizing influence of the outer conducting wall dominates that of the inner wall. The boundary condition $E_\theta = 0$ at the outer conducting wall may reduce the azimuthal component of the electric field at the electron beam, which is essential in the negative mass instability. As is shown in Fig. 10, this stabilizing effect is enhanced as the beam approaches to the outer conducting wall.[15]

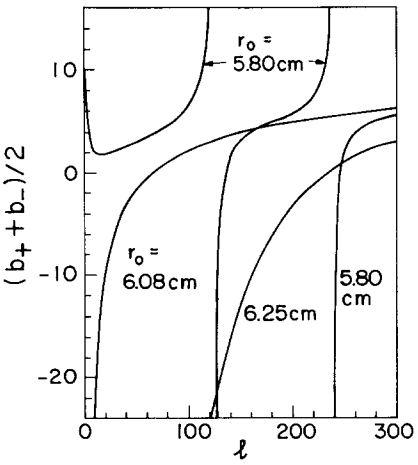

FIG. 10. The wave admittance $(b_+ + b_-)/2$ as a function of azimuthal mode number l, for $a = 6.51$ cm, $b = 5.40$ cm, $\gamma_0 = 5.1$, and varying electron-beam radii.

In our analysis in the text the growth rate of the negative mass instability is derived by setting $a_w = 0$ in the dispersion equation (55), yielding

$$\omega_i^2 = f_1(\omega_p^2/\gamma_0) - [\omega_0(\Delta\gamma/\gamma_0)]^2. \tag{A7}$$

This result is analogous to the result of Eq. (A2) in Uhm and Davidson.[14] Comparing the two equations yields f_1 as defined in Eq. (21) of the text. More recently we have examined the circular FEL utilizing a fluid model and have derived f_1 from first principles.

In Fig. 9 the growth rate has its peak for the $q = 2$ radial mode, with $l = 229$ at $r_0 = 6.08$ cm. We find $b_+ = 6.65$, $b_- = 4.29$ (close to $\gamma_0 = 5.1$), and $f_1 = 3.94$ from Eq. (21).

[1] G. Bekefi, Appl. Phys. Lett. **40**, 578 (1982).
[2] R. C. Davidson, W. A. McMullin, and K. Tsang, Phys. Fluids **27**, 233 (1984).
[3] Y. Z. Yin and G. Bekefi, Phys. Fluids **28**, 1186 (1985).
[4] G. Bekefi, R. E. Shefer, and W. W. Destler, Appl. Phys. Lett. **44**, 280 (1984).
[5] W. W. Destler, F. M. Aghmir, D. A. Boyd, G. Bekefi, R. E. Shefer, and Y. Z. Yin, Phys. Fluids **28**, 1962 (1985).
[6] N. M. Kroll, P. L. Morton, and M. N. Rosenbluth, IEEE J. Quantum Elect. **QE-17**, 1436 (1981).
[7] W. B. Colson, IEEE J. Quantum Elect. **QE-17**, 1417 (1981).
[8] D. Prosnitz, A. Szoke, and V. K. Neil, Phys. Rev. A **24**, 1436 (1981).
[9] R. Bonifacio, C. Pelligrini, and L. M. Narducci, Opt. Commun. **50**, 373 (1984).
[10] T. J. Orzechowski, E. T. Scharlemann, B. Anderson, V. K. Neil, W. M. Fawley, D. Prosnitz, S. Yarema, D. B. Hopkins, A. C. Paul, A. M. Sessler, and J. S. Wurtele, IEEE J. Quantum Elect. **QE-21**, 831 (1985).
[11] R. A. Waldron, *Theory of Guided Electromagnetic Waves* (Van Nostrand Reinhold, London, 1969).
[12] C. E. Nielson, A. M. Sessler, and K. R. Symon, in *Proceedings of the CERN Symposium on High Energy Accelerators* (European Organization for Nuclear Research, Geneva, 1959), p. 239.
[13] R. J. Briggs and V. K. Neil, Plasma Phys. **9**, 209 (1967).
[14] H. S. Uhm and R. C. Davidson, Phys. Fluids **20**, 771 (1977).

[15]D. Chernin and Y. Y. Lau, Phys. Fluids **27**, 2319 (1984).
[16]H. P. Freund, P. Sprangle, D. Dillenburg, E. H. da Jornada, R. S. Schneider, and B. Liberman, Phys. Rev. A **26**, 2004 (1982).
[17]H. P. Freund and P. Sprangle, Phys. Rev. A **28**, 1835 (1983).
[18]P. Sprangle, R. A. Smith, and V. L. Granatstein, *Infrared and Millimeter Waves* (Academic, New York, 1979), Vol. 1, pp. 279–327.
[19]L. S. Schuetz, E. Ott, and T. M. Antonson, Bull. Am. Phys. Soc. **30**, 1549 (1985).